Research Article

Development of cable-in-conduit conductor for ITER CS in Japan

H. Kajitani[1] · T. Hemmi[1] · T. Suwa[1] · Y. Takahashi[1] · K. Matsui[1] · N. Koizumi[1]

Abstract

The National Institutes for Quantum and Radiological Science and Technology has the responsibility to develop a cable-in-conduit conductor (CICC) for the ITER central solenoid (CS). Qualification tests of CICCs fabricated in the initial development stage were carried out at the SULTAN test facility; the superconducting performance (T_{cs} = current-sharing temperature) was found to be degraded by the repeated cyclic loading that simulates realistic ITER operating conditions. From destructive examination and neutron diffraction tests, this degradation appears to result from bending strain on the strands generated by electromagnetic forces. In response, the cabling of the CICC was optimized by shortening the twist pitch to make it stiffer against electromagnetic forces. No T_{cs} degradation of the optimized CICC was seen in the subsequent SULTAN test; further, a CS insert (CSI) test was performed at the CS model coil test facility, which included hoop strain for a more realistic simulation of ITER conditions. Good performance was also achieved in the CSI test.

Keywords ITER · Cable-in-conduit conductor · Superconducting magnet system · Central solenoid

1 Introduction

The International Thermonuclear Experimental Reactor (ITER) is an international project undertaken by China (CN), Europe (EU), India (IN), Korea (KO), the Russian Federation (RF), the United States (US), and Japan (JA) [1]; these members are responsible for the design and fabrication of the major components to be assembled into the ITER facility. An overview of ITER is shown in Fig. 1; plasma confinement in the device is based on a superconducting magnet system. All ITER members except IN contribute to the development. The ITER magnet system is the largest unified superconducting magnet system ever built in the world.

The superconducting magnet system [2, 3] consists of four different types of coils. These are 18 toroidal field (TF) coils, 6 poloidal field (PF) coils, 18 correction coils (CC), and 6 central solenoid (CS) modules, as shown in Fig. 2. These coils rely on cable-in-conduit conductors (CICCs) [4], which contain superconducting strands twisted in multiple stages in a stainless steel conduit. The conductors in

the TF and CS coils consist of Nb_3Sn strands, while the PF and CC conductors consist of Nb-Ti strands. These conductors are cooled by cryogenic fluids and operated below the current-sharing temperature (T_{cs}).

The National Institutes for Quantum and Radiological Science and Technology (QST), acting as Japan's domestic agency in ITER, has responsibility to develop the CS conductor [5, 6]. There are 49 conductors, each having the length of several hundred meters, which are to be produced for the CS. The operating scenario for the CS is pulsed operation that induces 15 MA of plasma, with 30,000 repetitions and a burn duration of 400 s [7]; the CS conductor must therefore survive severe repeated cycles of electromagnetic force (EM). A requirement of the CS conductor is no degradation of T_{cs} from the EM cycles.

In 2010 and 2011, qualification tests of the CS conductor initially developed were performed, showing unexpected degradation of T_{cs} in the EM cycles. Investigations were undertaken to understand this degradation [8, 9]; one of the most effective techniques was neutron diffraction
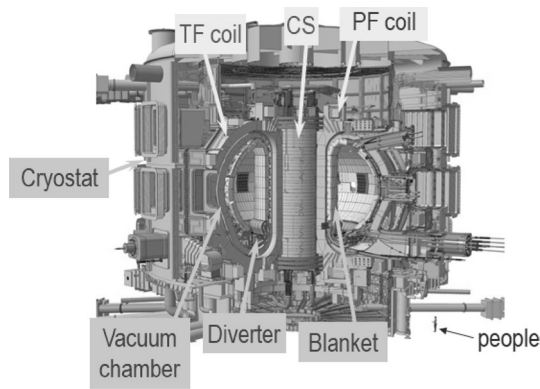
Fig. 1 Overview of ITER. CS designates the central solenoid; *TF* toroidal field, *PF* poloidal field
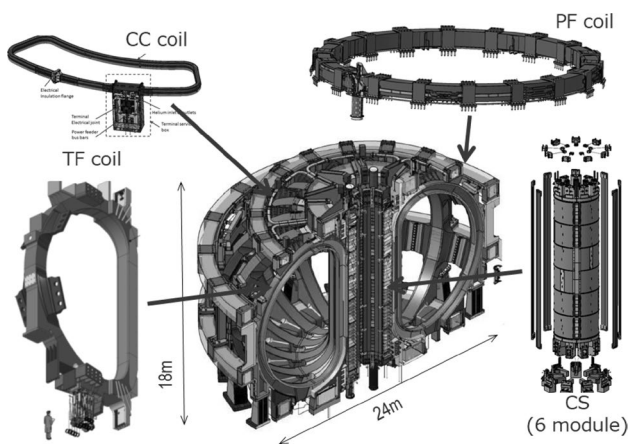
Fig. 2 ITER superconducting magnet system (TF, PF, CC coils, and CS)

analysis. This analysis clearly showed strand deformation [10] as the cause of the T_{cs} degradation; consequently, the authors decided to optimize the conductor design to prevent this deformation. The status of this work is described in this paper.

To re-design the conductor [11–13], the twist pitch of the cable was shortened. It was expected that a shorter twist pitch configuration would reduce the strand deformation under EM cycles; however, this optimization produced another problem: dented strands during the cabling process. To overcome this issue, QST improved the cabling process by applying empirical criteria to the dented strand [14]; an overview is presented in this paper.

In 2012, a qualification test of the optimized conductor with a shorter twist pitch was performed and showed no degradation of T_{cs} with EM cycles [15]. With this success, series production of the CS conductors could begin, and in parallel, to confirm the performance of the optimized short twist pitch conductor under conditions which more

precisely duplicate the ITER CS operation, a central solenoid insert (CSI) was tested in 2015. The results satisfied all the CS requirements with a sufficient margin for T_{cs} [16]. The status is also described in this paper.
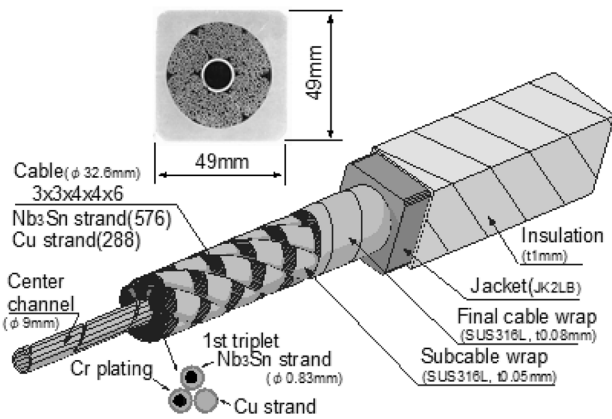
2 ITER CS conductor

The CS consists of 6 modules designated CS1U, CS1L, CS2U, CS2L, CS3U, and CS3L, as shown in Fig. 3. Each module has 40 layers of 6 hexa-pancake and 1 quadra-pancake. The hexa-pancake and quadra-pancake consist of 918 m and 613 m CIC conductor, respectively. Thus, a total of 49 CIC conductors are required for six modules plus one spare.

The CS is pulse-operated to produce 15 MA of plasma in the ITER scenario. Details of the scenario are shown in [7]. In this operation, the charge and discharge are repeated up to 30,000 cycles, and thus, the CS conductor is subjected to 60,000 repeated EM cycles. In this scenario, the conductor current is ramped up to 45 kA in a maximum field of 13 T. To accommodate this combination of high current and high magnetic field, the CS conductor consists of 576 Nb$_3$Sn and 288 copper strands, twisted in several stages and contained in a stainless steel conduit [7], as shown in Fig. 4. The conductor is cooled and should be operated below its current-sharing temperature, T_{cs}. Thus, the value of T_{cs} should remain above the operating temperature under repeated EM cycles. In the operation, there are two main critical conditions: One is the start-of-discharge (SOD), and the other is the end-of-burn (EOB) [7]. The SOD, with 40 kA of conductor current and 13 T of maximum field, presents the most severe conditions, that is, the smallest temperature margin; in comparison, the maximum EM force is applied during the EOB. Therefore,
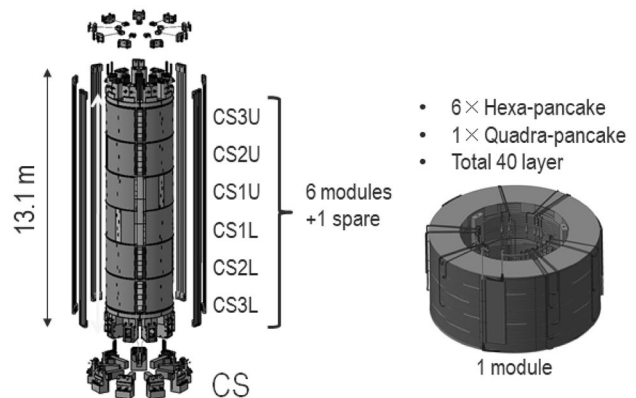
Fig. 3 Overview of central solenoid (6 modules). Each module contains 40 pancake layers

Fig. 4 ITER CS conductor center channel is for cooling; first twisted strand (triplet) contains two Nb₃Sn strands and one Cu strand; final stage of 6 strands shows the wrapping on each strand. In total, there are 576 Nb₃Sn strands and 288 copper strands

Fig. 5 Overview of SULTAN test and the conductor sample

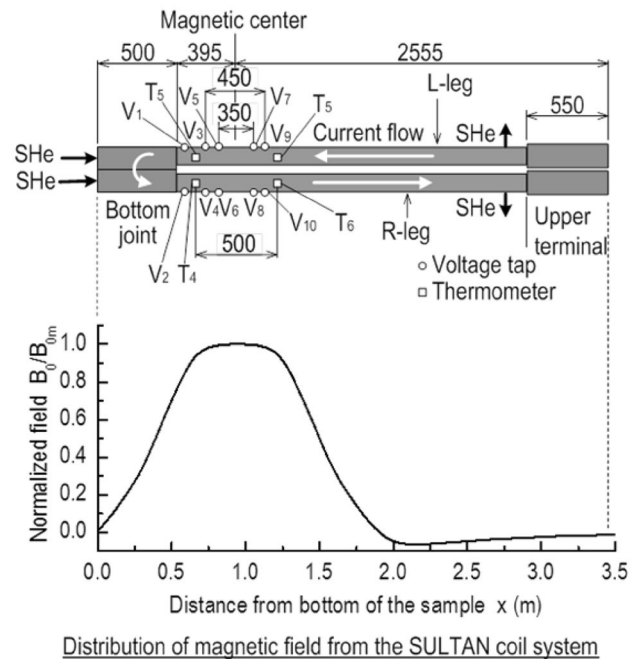the constraint on T_{cs} is defined by the SOD conditions; the limiting value for T_{cs} is 5.2 K.

3 Initial design of the CS conductor

The major parameters of the initial CS conductor are listed in Table 1; this design was based on previous reports [17, 18]. Nb₃Sn and Cu strands were twisted in five stages with 45, 85, 145, 250, and 450 mm pitch, with a center channel, and then inserted into a JK2LB 49 mm square stainless steel conduit. In the initial stage of the development, the qualification test was performed using the SULTAN test facility and will be denoted *the SULTAN test*. Its purpose was to determine whether the conductor satisfies the required T_{cs} through a number of EM cycles.

In the SULTAN test, two straight conductor samples of length about 3.5 m are positioned as shown in the test facility, which applies an external magnetic field (Fig. 5) [19]. The SULTAN test facility is the only way to confirm performance of ITER scale conductor. However, the peak external field is limited to 10.85 T, which corresponds to about 11.5 T of maximum field during conductor current

Table 1 Major parameters of the CS conductor initial design

Conductor	
Cabling layout	(2SC + 1Cu) × 3×4 × 4×6
Twist pitch	45/85/145/250/450 mm
Jacket material	JK2LB
Inner cable diameter	32.6 mm
Outer dimension	49 mm × 49 mm
Void fraction	34.3%

flow. Therefore, the current chosen for the T_{cs} measurements was 45 kA, which reproduces the EM force experienced during the SOD condition (i.e., SOD condition: 40 kA × 13 T ≃ SULTAN condition: 45 kA × 11.5 T), while EM cycle is done by 48.8 kA of sample current (EOB condition) [4]. As the external field in the SULTAN test condition is different from that during SOD, the T_{cs} criterion was adjusted to 6.5 K for the test.

To measure the current-sharing temperature T_{cs}, the voltage of the sample was monitored as its temperature was increased, while maintaining the test conditions of 45 kA and 11.5 T. T_{cs} is defined as the temperature when the voltage reaches 10 μV/m. The T_{cs} measurement was repeated through the test, allowing the T_{cs} dependence on number of EM cycles to be determined (Fig. 6). T_{cs} decreases linearly with the number of EM cycles and is extrapolated to fall below the criterion of 6.5 K at around 12,000 cycles. Thus, the initial conductor design is clearly not appropriate for the CS conductor.

4 Consideration of the degradation

To investigate the SULTAN test results seen in Fig. 6, which shows an unexpected level of T_{cs} degradation with EM cycles, a destructive examination (DE) was done on the sample tested. A visual inspection of a section of cable surface was carried out to investigate the effects of the large EM forces applied; the observations were specifically
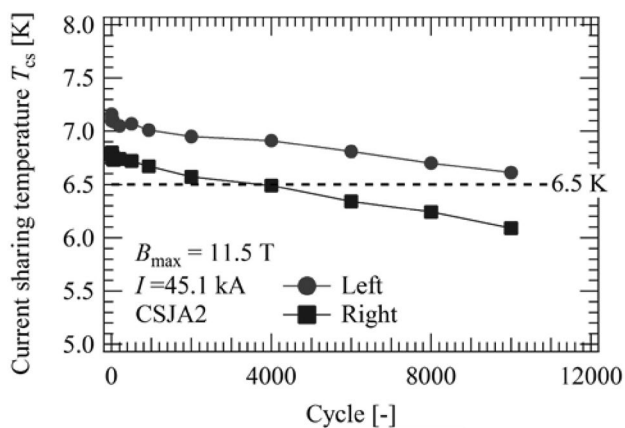
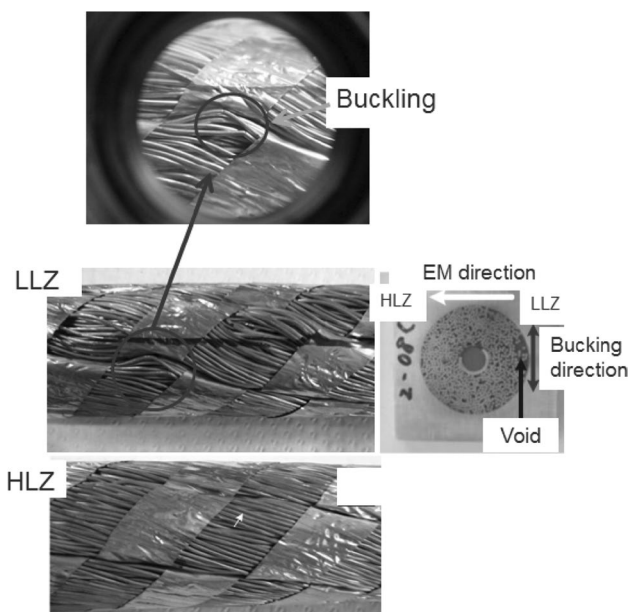**Fig. 6** Current-sharing temperature T_{cs} for the initial conductor design, as a function of EM cycles

directed at the high-load zone (HLZ) and the low-load zone (LLZ). The inspection showed that strands in the LLZ exhibited the most bending (Fig. 7). Because the direction of the bent strand did not correspond to that of the EM loading, another cause was sought; the original assumption had been that strand bending was only caused by EM loading in the HLZ [20, 21]. Thus, the observed phenomenon required a more complex explanation.

Researchers have tried to understand this unexpected strand deformation in the LLZ [9, 22]; one mechanism was assumed: strand buckling. In this mechanism, thermal compressive forces originally acted on strands inside the conduit as a result of differences between the thermal

contraction properties of materials in the conductor, operating during the heat treatment and cool-down process. On the other hand, a large void was generated in the LLZ because EM loading pushed strands forward toward the HLZ. Since the large void allows strands to move easily, strands were compressed and then buckled by the thermal compressive forces, and as a result, strand buckling occurs in the LLZ [23].

To study the bent strand condition more quantitatively, various approaches were taken [9, 22, 23]. One of the most sophisticated studies used neutron diffraction analysis [10], which accurately evaluates strains in the strands inside the conductor. Figure 8 shows schematically the response of a neutron diffraction profile for the cases of axial or bending strain. If axial strain occurs, the diffraction peaks are shifted, while if bending strain occurs, the diffraction profile is broadened.
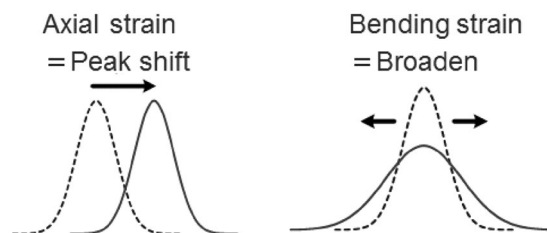
The neutron diffraction analysis was performed for SULTAN test samples from the HLZ, the LLZ, and a low-field zone (LFZ) where the external field is almost zero. Since the LFZ is exposed to a sufficiently small electromagnetic force, it is assumed there is no degradation. The result is shown in Fig. 9. The diffraction profile from the LLZ is much broader than the other profiles. This clearly shows that strands in the LLZ bent the most severely. Since Nb_3Sn strands are very sensitive to strain, it was concluded that the main cause of conductor degradation shown in Fig. 6 was strand deformation such as buckling and/or bending in the LLZ.

5 Optimized conductor design

To prevent the strand deformations in the LLZ mentioned in the last section, research and development on the cable configuration was undertaken [11–13]. The main approach chosen for optimization was to shorten the twist pitch of the cable to 20, 45, 80, 150, and 450 mm in the stages, as shown in Fig. 10. It was expected that the short twist pitch (STP) configuration would reduce the strand deformation

Fig. 7 Cable surface in the LLZ and HLZ observed in destructive examination of the SULTAN test sample

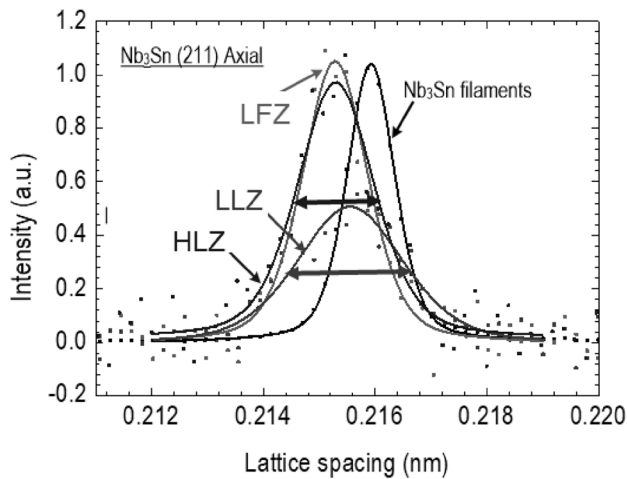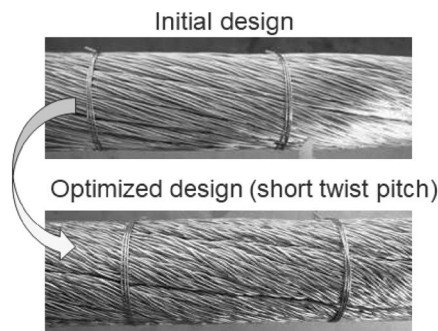**Fig. 8** Response of a neutron diffraction profile for axial or bending strain

Fig. 9 Neutron diffraction analysis for high-load zone (HLZ), low-load zone (LLZ), and low-field zone (LFZ) SULTAN test samples

Fig. 10 Optimized short twist pitch conductor design

Fig. 11 Strand deformation during the cabling process

Fig. 12 Results of I_c measurement on dented strands. The horizontal axis is the depth of indentation, and the vertical axis shows I_c normalized to the undented value

new result gave the authors an empirical criterion for cable production. Based on this observation, the parameters of the cabling machine can be optimized so that harmful deformation of strands is avoided.

To confirm this effect in the STP-modified conductor, the SULTAN test was performed under the same conditions as in Fig. 6, with the results shown in Fig. 13 [13]. No degradation was observed through the same number of EM cycles, and it is concluded that this STP conductor design is appropriate for the CS conductor. Following the success of this development, series production of CS conductors was started.

6 CS insert test

Following the success of the SULTAN test with the optimized STP conductor, the series production of CS conductors could be started, as mentioned above. In

under EM cycles (seen in Fig. 7) because each strand is more tightly fixed inside a cable with a lower void fraction.

However, this optimization approach produced another problem for the cable production process. Destructive examination of the modified (i.e., STP) conductor sample revealed severe strand cross-sectional deformation inside the cable, as shown in Fig. 11 [14]. This deformation occurred during the cable manufacturing process, as a result of each strand being more tightly twisted and compacted. To assess the influence of this deformation on strand performance, critical current (I_c) measurements on dented strands were performed (Fig. 12). From these measurements, I_c can be kept to 95% of its value if the dents are smaller than 0.21 mm; this
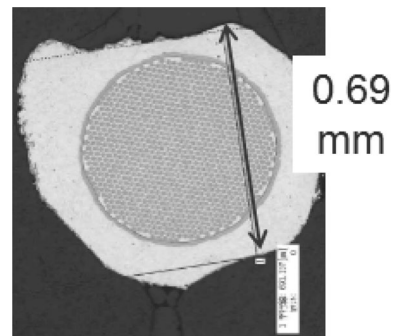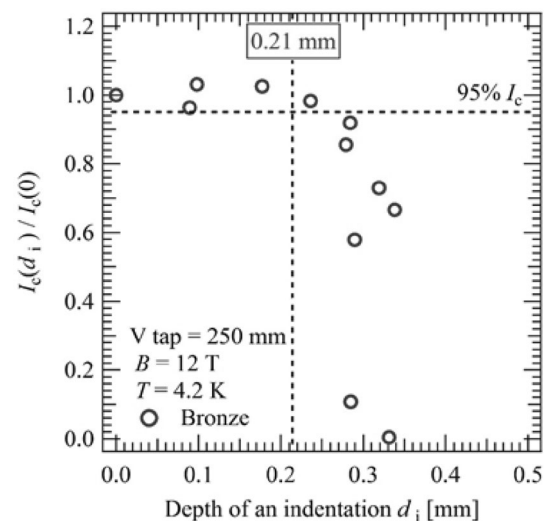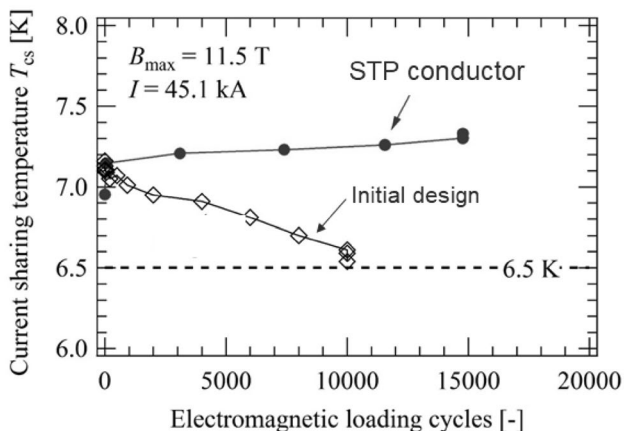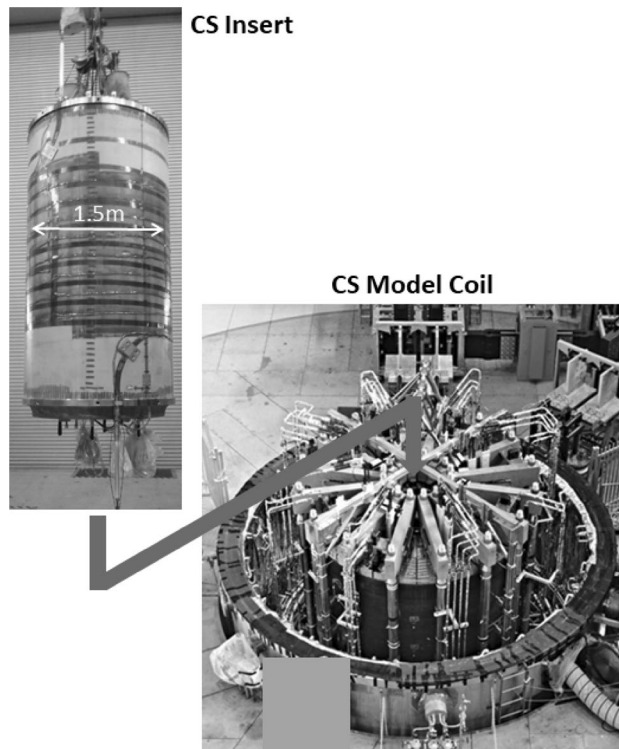
Fig. 13 Measurement results of T_{cs} as a function of EM cycles in the optimized short twist pitch conductor

Fig. 14 Overview of the CS insert (CSI) test at the CS Model Coil Facility

parallel, to finally check the performance of the STP conductor under conditions which are more precisely the same as during CS operation, a central solenoid insert sample (CSI) was tested in the external field of the Central Solenoid Model Coil (CSMC) Facility [17] shown in Fig. 14.

As the CSI is a single-layer solenoid, strain induced by the circular geometry (hoop strain) can be included in the evaluation of the CS conductor performance, which is not possible in the straight-line conductor samples in the SULTAN test. In addition, CSMC can generate an external field up to 13 T. Thus, the purpose of the CSI test is to evaluate T_{cs} under real CS operation (i.e., SOD conditions: 13 T of external field and 40 kA of current) with hoop strain. An additional objective was to compare the results to the SULTAN tests. Therefore, the CSI tests also included the SULTAN conditions of 11.5 T of external field and 45 kA of current. The requirement criteria for T_{cs} are 5.2 K and 6.5 K in the SOD and SULTAN conditions, respectively, as discussed above.

The result of the CSI test with SOD conditions is shown in Fig. 15. No degradation of T_{cs} with increasing EM cycles was observed, and there was a temperature margin of at least 1.5 K above the 5.2 K of the requirement criterion. Thus, it can be assumed that even if 60,000 cycles of EM loading are imposed on the conductor, its performance will be sustained.
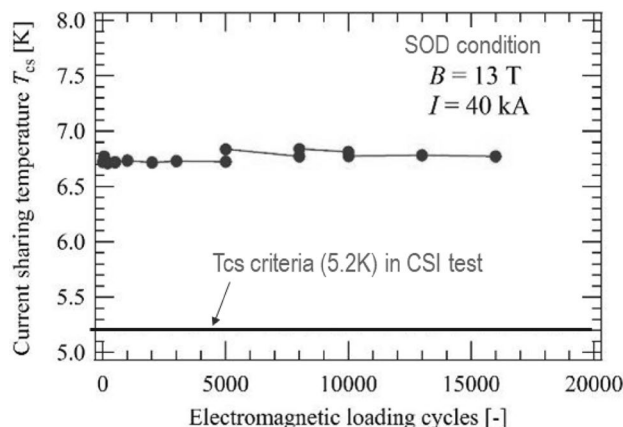
The CSI test result under SULTAN conditions is shown in Fig. 16. Again, no degradation of T_{cs} was observed and there is a sufficient temperature margin above the 6.5 K criterion for SULTAN conditions. In addition, the T_{cs} was about 0.5 K higher than the SULTAN test; this increase was the result of hoop strain. Thus, correlation between CSI and SULTAN tests was reasonable. This implies that the SULTAN test correctly represents the conductor performance.

7 Conclusion

Development of the CS conductor for ITER has given rise to technical challenges. However, QST overcame these difficulties with novel, accurate, and sophisticated investigation, notable consideration of the mechanisms degrading the current-sharing temperature and development of a

Fig. 15 Central solenoid insert (CSI) measurement of T_{cs} under SOD conditions, as a function of EM cycles
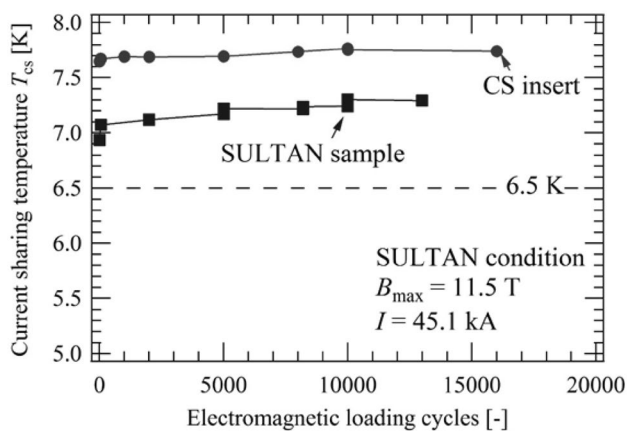
Fig. 16 CSI measurement of T_{cs} under SULTAN conditions, as a function of EM cycles, in comparison with the SULTAN conductor test result

Fig. 17 Group photograph after fabrication of the final conductor

short twist pitch design for the CS conductor. Following this successful development stage, the series CS conductor production could be started in 2012. In parallel, a final check to qualify the conductor performance (CSI test) was conducted in 2015. Fabrication of all the CS conductors was successfully completed in 2017; the photograph of completion of the final conductor is presented in Fig. 17. CS conductors were shipped to the USA, which is a coil manufacturer of the CS. The last conductors finally arrived in March 2018.

Compliance with ethical standards

Conflict of interest The authors declare that they have no conflict of interest.

Human and animals rights No human participant and animal were involved in this study.

References

1. Hotkamp N (2007) An overview of the ITER project. Fusion Eng Des 82:427–434
2. Sborchia C et al (2014) The ITER magnet systems: progress on construction. IAEA Nucl Fusion 54:013006
3. Mitchell N et al (2017) The ITER magnet system: configuration and construction status. Fusion Eng Des 123:17–25
4. Devred A et al (2012) Status of ITER conductor development and production. IEEE Trans Appl Supercond 22:4804909
5. Nabara Y et al (2013) Examination of Nb_3Sn conductors for ITER central solenoids. IEEE Trans Appl Supercond 23(3):4801604
6. Nabara Y et al (2016) Performance analysis of mass-produced Nb_3Sn conductor for central solenoid in ITER. IEEE Trans Appl Supercond 26(3):4200705
7. Devred A et al (2013) Conductor qualification program for the ITER central solenoid. IEEE Trans Appl Supercond 23:6001208
8. Bruzzone P et al (2012) Test results of ITER conductors in the SULTAN facility. In: Proceedings of 24th IAEA Fusion Energy Conference IAEA CN-197, p 536
9. Hemmi T et al (2012) Test results and investigation of Tcs degradation in Japanese ITER CS conductor sample. IEEE Trans Appl Supercond 22:4803305
10. Hemmi T et al (2013) Neutron diffraction measurement of internal strain in the first Japanese ITER CS conductor sample. Supercond Sci Technol 26:084002
11. Bessette D (2014) Design of a Nb_3Sn cable-in conduit conductor to withstand the 60,000 electromagnetic cycles of the ITER central solenoid. IEEE Trans Appl Supercond 24:4200505
12. Nijhus A (2011) Optimization of ITER Nb_3Sn CICCs for coupling loss, transverse electromagnetic load and axial thermal contraction. Supercond Sci Technol 25:015007
13. Nabara Y et al (2014) Impact of cable twist pitch on Tcs degradation and AC loss in Nb_3Sn conductors for ITER central solenoids. IEEE Trans Appl Supercond 24:4200705
14. Takahashi Y et al (2014) Cabling technology of Nb_3Sn conductor for ITER central solenoid. IEEE Trans Appl Supercond 4:4802404
15. Devred A et al (2014) Challenges and status of ITER conductor production. Supercond Sci Technol 27:044001
16. Martovetsky N et al (2016) ITER central solenoid insert test results. IEEE Trans Appl Supercond 26(4):4200605
17. Tsuji H et al (2001) ITER R&D magnets: central solenoid model coil. Fusion Eng Des 55:153–170
18. Martovetsky N et al (2002) Test of the ITER central solenoid model coil and CS insert. IEEE Trans Appl Supercond 12:600–605
19. Bruzzone P et al (2002) Upgrade of operating range for SULTAN test facility. IEEE Trans Appl Supercond 12:520–523
20. Nunoya Y (2004) Experimental investigation on the effect of transverse electromagnetic force on the V-T Curve of the CIC conductor. IEEE Trans Appl Supercond 14(2):1468–1472
21. Koizumi N (2006) A new model to simulate critical current degradation of a large CICC by taking into account strand bending. IEEE Trans Appl Supercond 16(2):831–834
22. Sanabria C et al (2012) Evidence that filament fracture occurs in an ITER toroidal field conductor after cyclic Lorentz force loading in SULTAN. Supercond Sci Technol 25:075007
23. Kajitani H et al (2013) Analytical study of degradation of CIC conductor performance due to strand bending and buckling. IEEE Trans Appl Supercond 23:2247652